Icarus 253 (2015) 130–141

Contents lists available at ScienceDirect

Icarus

journal homepage: www.elsevier.com/locate/icarus

A search for SO_2, H_2S and SO above Tharsis and Syrtis volcanic districts on Mars using ground-based high-resolution submillimeter spectroscopy

A.S. Khayat [a,*], G.L. Villanueva [b,c], M.J. Mumma [b], A.T. Tokunaga [a]

[a] Institute for Astronomy, University of Hawaii, Honolulu, HI 96822, USA
[b] Solar System Exploration Division, Mailstop 690, NASA Goddard Space Flight Center, Greenbelt, MD 20771, USA
[c] Department of Physics, Catholic University of America, Washington, DC 20064, USA

ARTICLE INFO

Article history:
Received 23 August 2014
Revised 11 February 2015
Accepted 27 February 2015
Available online 10 March 2015

Keywords:
Mars, atmosphere
Abundances, atmospheres
Atmospheres, structure
Radiative transfer
Volcanism

ABSTRACT

We surveyed the Tharsis and Syrtis volcanic regions on Mars during 23 November 2011 to 13 May 2012 which corresponded to its mid Northern Spring and early Northern Summer seasons (L_s = 34–110°). Strong submillimeter rotational transitions of sulfur dioxide (SO_2), sulfur monoxide (SO) and hydrogen sulfide (H_2S) were targeted. No active release was detected, and we infer 2σ upper limits across the disk of the planet of 1.1 ppb, 0.7 ppb and 1.3 ppb for SO_2, SO and H_2S, respectively. Our derived upper limit for SO_2 is comparable to previously reported limits, whereas for H_2S we set a more stringent upper limit than previously measured, and we establish a limit for SO. Among the targeted molecules, SO_2 is the strongest indicator for volcanic outgassing. Assuming a photochemical lifetime of 2 years for SO_2, our upper limit of 1.1 ppb implies an outgassing rate less than 55 metric tons/day. This rate limits the daily amount of degassing magma to less than 12,000 m^3. Our sensitivity is sufficient to detect a volcanic release on Mars that is 4% the SO_2 released continuously from Kilauea volcano in Hawaii or 5% that of the Masaya volcano in Nicaragua. The non-detection of the sulfur compounds in the atmosphere of Mars indicates the absence of major volcanic outgassing.

1. Introduction

The study of planetary atmospheres by means of spectroscopy is important for understanding their origin and evolution. The presence of short-lived trace gases in the martian atmosphere would have implications for recent ongoing geologic activity on the planet.

The size–frequency distribution of craters on the surface of Mars is an indicator of the age of martian volcanoes. The crater number density on old surfaces is higher compared to new ones, owing to the fact that time allowed more craters to form on old surfaces. Robbins et al. (2011) analyzed images from the Mars Reconnaissance Orbiter's ConTeXt Camera (CTX), in order to constrain the time since volcanoes on Mars were last active. By targeting calderas of 20 major volcanoes on Mars, they inferred a volcanic activity in Tharsis ending around 150 Myr ago. Using the High Resolution Stereo Camera (HRSC) onboard Mars Express, Neukum et al. (2004) applied cratering chronology models to investigate the geologic evolution of two focal points of volcanism on Mars: Tharsis province and Elysium area. They identified 5 different calderas on Ascraeus Mons with intermittent volcanic activities that occurred around 100 Myr, 200 Myr, 400 Myr, 800 Myr and 3.6 Gyr. As a consequence of prolonged episodic volcanic activity, Neukum et al. (2004) suggested that volcanoes in Tharsis may still be outgassing, even today. Werner (2009) who also used HRSC, was able to confirm the earlier measurements of Neukum et al. (2004), and suggested that volcanic activity on the planet ended up being localized in Tharsis, with recent volcanism occurring to about 100–200 Myr ago. Hauber et al. (2010) investigated plain-style volcanism in Tharsis using CTX and determined the ages of 60 volcanoes and lava flows. They dated clusters of low shield volcanoes to ages <100 Myr.

The possibly long lifetime of volcanoes on Mars, extending to 2–3 billion years in the case of Olympus Mons, although intermittent, is exceptional among volcanoes in the Solar System (Frankel, 1996). Such longevity increases the probability of finding active vents that might be present on Mars today. In addition, images from the Mars Global Surveyor helped Hartmann et al. (1999) to refine the results of crater count statistics by studying crater sizes

* Corresponding author.
E-mail address: Khayat@ifa.hawaii.edu (A.S. Khayat).

http://dx.doi.org/10.1016/j.icarus.2015.02.028
0019-1035/Published by Elsevier Inc.

down to 16 m. The wide range of surface ages indicated by their results suggests a continuous process of volcanism that could be extending to the current geological time.

Even though recent active volcanism on Mars has not yet been found (Edgett et al., 2010), the presence of local outgassing vents may be possible. Outgassing from local vents could temporarily alter the composition and disrupt the equilibrium of its atmosphere (Wong et al., 2003). Methane release on Mars, in either mid-summer in the northern hemisphere in 2003 or early spring in the southern hemisphere in 2005, may have occurred from subsurface warming or opening in scarps or crater walls (Mumma et al., 2009).

By analogy with the Earth (Symonds et al., 1994), volcanic outgassing includes sulfur compounds such as sulfur dioxide (SO_2), hydrogen sulfide (H_2S) and sulfur monoxide (SO), a major photochemical product (Wong et al., 2005, 2004, 2003). Models by Gaillard and Scaillet (2009) show that the volcanic gases released from martian volcanoes during formation of the Tharsis region were 10–100 times richer in sulfur compared to the gases released from volcanoes on Earth. Since SO_2 is the main gas released among the other sulfur gases (Andres et al., 1991), its absence places a sensitive limit on the volcanic outgassing on Mars, today.

To test for such outgassing, it is necessary to search for H_2S and SO, along with SO_2. Measuring the chemical composition of the gas flux gives important clues about the magma and its volatile content, its behavior, and the dynamics of degassing under martian conditions. In Earth's volcanoes, the SO_2/H_2S ratio generally varies between 10^{-1} and 3×10^2. Measuring the relative proportions of the sulfur species is essential for understanding local conditions in the magma chambers where these species form, because the SO_2/H_2S ratio is dictated by the local pressure and temperature (Oppenheimer et al., 2011; Delmelle and Stix, 2000).

In an attempt to estimate the abundance of sulfur compounds released into the atmosphere of Mars, Wong et al. (2003, 2004, 2005) developed a photochemical model. They considered outgassing of H_2S and SO_2 from possible hot spots. After being released into the atmosphere, a fraction of the molecules is photo-dissociated, another fraction reacts with other species in the atmosphere, and the remainder gets recycled. Assuming an initial local abundance ratio at the surface of 100 ppm for the released H_2S and SO_2, the computed lifetime, or time it takes each species to be removed photochemically, is 600 days for SO_2 (Wong et al., 2005), 9 days for H_2S, and 4.6 h for SO (Wong et al., 2003, 2005). An additional motivation to look for SO and H_2S along with SO_2 is that their relative abundance better constrains the photochemical cycle involving sulfur species during an outgassing event of volcanic origin.

In case of a one-time outgassing event on Mars, the lifetime of SO_2 requires a search that must span multiple seasons and years in order to constrain episodic or occasional release. In the case of a steady state outgassing, the number of molecules in the atmosphere above the outgassing source reaches an equilibrium state. Since the lifetime of SO_2 in the martian atmosphere is larger than the global mixing timescale of 0.5 year (Krasnopolsky et al., 2004), we can consider the molecules to be well mixed across the planet, and no major seasonal changes will be observed. Assuming they are correct, the short lifetimes of H_2S and SO do not allow the molecules to be globally mixed across the planet, and one should then assume a release of these molecules from a global distribution of sources on Mars in order to have a detection. SO_2, H_2S and SO do not condense at the atmospheric conditions above the seasonal polar caps.

H_2S and SO ro-vibrational transitions in the infrared are generally weak (Rothman et al., 2009). SO_2 has a strong band centered at 7.34 μm, but Earth's atmosphere is almost opaque at this wavelength. However, the strengths of rotational transitions of SO_2, H_2S and SO in the submillimeter, combined with Earth's high atmospheric transmission at the specific wavelengths, make it possible to achieve a sensitive search for the volcanic molecules. Therefore, one of the best ways to detect the molecules is through their rotational spectra (Encrenaz et al., 2004), using a large single dish antenna such as the Caltech Submillimeter Observatory (CSO).

Earlier ground-based attempts to detect gaseous sulfur species in the atmosphere of Mars were unsuccessful. SO_2 was searched at 7.4 μm using the Texas Echelon Cross Echelle Spectrograph (TEXES) at the NASA Infrared Telescope Facility (IRTF). In order to compensate for the low signal-to-noise ratio caused by the opacity of Earth's atmosphere around this wavelength, Encrenaz et al. (2011) and Krasnopolsky (2012) co-added the spectra spatially and spectrally at nine selected transitions, and obtained a similar stringent upper limit of 0.3 ppb at 2σ. Encrenaz et al. (1991) looked for H_2S in the millimeter at the $J_{n,k} = 2_{2,0} - 2_{2,1}$ transition at 216.71 GHz, and found an upper limit of 20 ppb for the mixing ratio. SO was not looked for and therefore there is no upper limit for it.

In this paper we describe new and extensive submillimeter searches for SO_2, H_2S and SO above the Tharsis and Syrtis volcanic regions. Our work is motivated by the possibility of detecting current outgassing and improving the limits of sulfur species in the atmosphere of Mars. In Section 2 we present our observations. In Section 3 we explain the methodology in retrieving the thermal structure and brightness temperature of Mars at the time of the observations, and describe the radiative transfer model that we used to retrieve the abundances. We report disk-averaged (2σ) upper limits for SO_2, SO and H_2S in Section 4. The results are discussed in Section 5, and summarized in Section 6.

2. Observations

We used the double side band high resolution heterodyne receiver "Barney" (Kooi et al., 2007) at the 10.4 m single dish antenna of the CSO on Mauna Kea, Hawaii, to look for several sulphuretted species: SO_2 ($J_{n,k} = 19_{1,19} - 18_{0,18}$) at 346.652 GHz, H_2S ($J_{n,k} = 3_{3,0} - 3_{2,1}$) at 300.505 GHz and SO ($J_n = 7_8 - 6_7$) at 304.077 GHz (Pickett et al., 1998). The targeted volcanic areas, Tharsis and Syrtis Major, were observed during the interval 23 November 2011–13 May 2012 spanning mid Northern Spring and early Northern Summer seasons, between $L_s = 34°$ and $L_s = 110°$ in Mars year 31 (MY 31). We observed Syrtis at longitudes ranging from 222°W to 345°W, and Tharsis from longitude 48°W to 177°W, both regions at the respective sub-Earth point when measured. The angular size of Mars changed between 6.7 and 9.0 arcsec on the first and the last run, respectively. The observing parameters are given in Table 1.

The tapered beam of the CSO at 346.5 GHz has a FWHM of 24.3 arcsec.[1] The geocentric velocity for Mars ranges between −15.41 km/s and +13.71 km/s. The Earth's atmospheric transmission, $\exp(-\tau)$, at the SO_2 frequency setting is lower than at the SO and H_2S, therefore more signal from Mars is absorbed by Earth's atmosphere, leading to a lower signal-to-noise ratio at the continuum around the SO_2 transition. In order to compensate for that, SO and H_2S were searched for under normal weather conditions at a telluric optical depth at 225 GHz, $\tau_{225\ GHz} < 0.14$,[2] and SO_2 was searched under excellent submillimeter conditions with $\tau_{225\ GHz} < 0.1$. $\tau_{225\ GHz}$ refers to opacity as introduced by water vapor, and since there is a significant water absorption at the observed frequencies (300–350 GHz), low opacity levels at 225 GHz produces excellent transmission at the SO_2 transition.

[1] http://www.submm.caltech.edu/cso/receivers/beams.html.
[2] http://cso.caltech.edu/tau/.

Table 1
Parameters for Mars during the observing dates.

Target line	Frequency (GHz)	Date (UT)	Heliocentric velocity (km/s)	Geocentric velocity (km/s)	Angular size (arcsec)	L_s (°)	Integration time (min)
SO_2	346.652	28 November 2011	1.3	−15.6	6.9	36	67
SO_2	346.652	22 January 2012	0.4	−13.1	10.9	60	93
SO_2	346.652	23 January 2012	0.4	−13.0	11.0	61	89
SO_2	346.652	21 April 2012	−1.1	12.3	10.7	100	71
SO_2	346.652	22 April 2012	−1.1	12.4	10.6	101	62
SO_2	346.652	23 April 2012	−1.1	12.6	10.6	101	67
SO_2	346.652	08 May 2012	−1.3	13.6	9.4	107	53
SO_2	346.652	09 May 2012	−1.3	13.6	9.3	108	59
SO	304.078	27 November 2011	1.3	−15.6	6.91	34	56
SO	304.078	18 January 2012	0.5	−13.7	10.5	59	72
SO	304.078	19 January 2012	0.5	−13.6	10.61	59	86
SO	304.078	20 April 2012	−1.1	12.2	6.91	99	50
SO	304.078	24 April 2012	−1.1	12.7	6.91	101	52
SO	304.078	10 May 2012	−1.4	13.7	6.91	108	57
SO	304.078	11 May 2012	−1.4	13.67	9.15	108	50
H_2S	300.505	29 November 2011	1.3	−15.7	7.0	36	60
H_2S	300.505	20 January 2012	0.4	−13.4	10.7	59	96
H_2S	300.505	21 January 2012	0.4	−13.3	10.8	60	97
H_2S	300.505	25 April 2012	−1.1	12.7	10.4	102	65
H_2S	300.505	26 April 2012	−1.2	12.8	10.3	102	61
H_2S	300.505	12 May 2012	−1.4	13.7	9.1	109	47
H_2S	300.505	13 May 2012	−1.4	13.7	9.0	110	39

The accuracy in the pointing of the telescope was checked on shorter time intervals at the beginning of the night and before sunrise when there are considerable changes in the telescope temperature.[3] During the night, the continuum source pointing using Mars was done every 1.5–2 h by making a five-point map around the planet. Chopping between Mars and the sky at 60 arcsec from the planet was achieved by wobbling the secondary mirror of the telescope.[4] We used the chopper-calibration method (Penzias and Burrus, 1973) to calibrate the antenna temperature. The major contributions to the systematic errors in the antenna temperature are the pointing and focussing of the telescope, the double side band ratio, the tuning of the receivers and the variations in the atmospheric transmission (Matthews et al., 2004). As a result, variations in the baseline are expected. The calculated uncertainties resulting from each contributing factor were later added quadratically. The resulting estimated systematic uncertainty for these nights was ∼15% of the continuum level. Examples of the observed spectra at the SO_2, SO and H_2S settings for April, 23, 24 and 25 UT, 2012, respectively are displayed in Fig. 1.

The antenna temperature of Mars continuum depends on the telescope's efficiency, beam width at the frequency setting, the size of Mars and the ratio of contributions from the receiver's lower and upper side bands. For one night, we measured the double-side-band ratio, and found equal contributions from both side bands. The same ratio is considered for the rest of the nights.The slight shifts at the continuum level in Fig. 1 among the three different settings are within the systematic uncertainty from night to night. The error bars presented in the spectra are the RMS noise level of the continuum.

As a sanity check to see if there is anything blocking the beam, we pointed the telescope to Orion KL and confirmed the presence of the SO_2 and SO emission lines (Schilke et al., 1997), their transition frequency, and antenna temperature. In the Mars data, the variations in the baseline were later corrected for the data analysis, by using polynomial fitting. For each night, the expected noise level in the spectra was calculated from the system temperature using the radiometer equation (Encrenaz et al., 1995), and it was found to be consistent with the measured noise. For example, on January 23 UT, 2012, with a system temperature of 384 K, a spectral resolution of 1 MHz, a total integration time of 2.6 min, a Mars brightness temperature of 210.4 K, a filling factor of 0.132, a beam efficiency of 0.65 and a beam-switching observing mode, the measured noise is 69.4 mK, compared to the expected noise of 67.2 mK.

At the SO_2 setting, the spectrometer's 4 GHz bandwidth covers the ^{12}CO(3-2) transition at 345.795 GHz. This ^{12}CO is later used to retrieve the thermal structure and the physical conditions in the martian atmosphere on the nights when we searched for SO_2. We used the Array Acousto Optic spectrometer (AOS) to measure the CO line shape. The array is divided into 4 individual sections covering 1 GHz each, with 2048 channels (650 kHz spacing) and a spectral resolution of 1 MHz (spectral resolving power ∼346,000) (Horn et al., 1999).

3. Method

3.1. A priori Mars brightness temperature

Local temperatures on Mars respond to insolation and vary according to surface albedo. We estimated the disk-integrated brightness temperature using a simple map based on these two parameters and the surface emissivity. We extracted the albedo map obtained by the Mars Global Surveyor's Thermal Emission Spectrometer (Christensen et al., 2001) and created a two dimensional orthographic projection. The benefit from using such projections is that this method takes into account the sizes of the different projected areas of the surface elements on Mars, as a weighting factor.

The disk is divided into a square grid of 90 × 90 equal-sized bins. The surface temperature at the center of each bin is calculated using the Mars Climate Database (MCD) (Lewis et al., 1999; Forget et al., 1999). By centering a two dimensional gaussian kernel (the normalized telescope beam) at the disk of Mars, the average brightness temperature for the whole planet at the time of the observations is calculated using the following equation:

$$\overline{T_b} = \epsilon_0 \times \frac{\sum_i \mathrm{Kernel}_i \times \mathrm{Mask}_i \times T_i}{\sum_i \mathrm{Kernel}_i \times \mathrm{Mask}_i} \quad (1)$$

where ϵ_0, Kernel, Mask and T are the emissivity of Mars at the observing frequency range, the values of the contribution from

[3] http://cso.caltech.edu/wiki/cso/instruments/heterodyne/pointing.
[4] http://cso.caltech.edu/wiki/cso/instruments/heterodyne/chop.

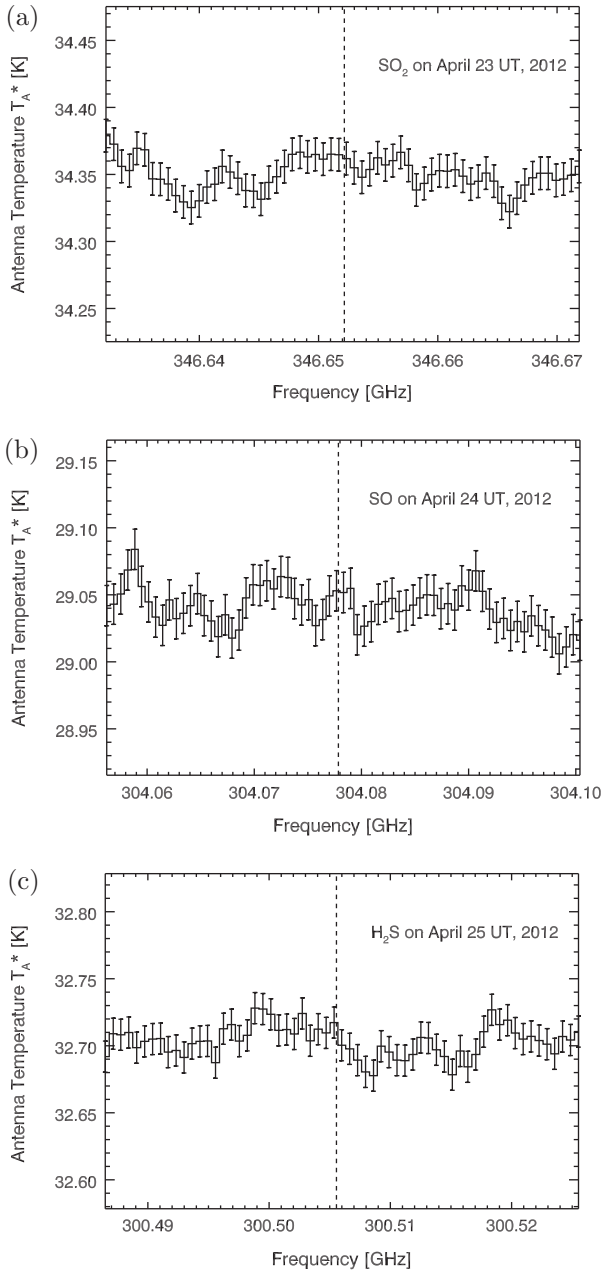

Fig. 1. Examples of summed double side band spectra of SO_2, SO and H_2S on April 23, 24 and 25 UT, 2012, respectively. The spectra are presented near rest frequencies (dashed lines) of the lines at 346.652 GHz, 304.078 GHz and 300.505 GHz, respectively. The error bars are the RMS uncertainty of the continuum.

the CSO gaussian beam, the mask (1 for the bins inside the martian disk, 0 elsewhere) and the surface temperature at each bin, respectively.

The emissivity of Mars is related to the Fresnel coefficient R, $\epsilon_0 = 1 - R$, which depends on the emission angle and the properties of the martian surface: the surface roughness and the dielectric constant ϵ. For a typical soil, the dielectric constant ranges between 2 and 3. Radar observations of the martian surface give values closer to 2 (Simpson et al., 1992; Golombek et al., 2008). We therefore adopt $\epsilon = 2.25$. The Fresnel coefficient of the polarized light has a parallel and a perpendicular component, $R = (R_s + R_p)/2$, where:

$$R_s = \left| \frac{n_1 \cos\theta_i - n_2 \sqrt{1 - \left(\frac{n_1}{n_2}\sin\theta_i\right)^2}}{n_1 \cos\theta_i + n_2 \sqrt{1 - \left(\frac{n_1}{n_2}\sin\theta_i\right)^2}} \right|^2 \quad (2)$$

$$R_p = \left| \frac{n_1 \sqrt{1 - \left(\frac{n_1}{n_2}\sin\theta_i\right)^2} - n_2 \cos\theta_i}{n_1 \sqrt{1 - \left(\frac{n_1}{n_2}\sin\theta_i\right)^2} + n_2 \cos\theta_i} \right|^2 \quad (3)$$

n_1 and $n_2 = \sqrt{\epsilon}$ are the indices of refraction for the air on Mars and the martian regolith, respectively, and θ_i is the incidence angle. The emissivity is flat at emission angles up to 25°, and is $\epsilon_0 = 0.96$. This number is used in our radiative transfer model.

3.2. Thermal structure retrieval

The optically thick martian CO(3-2) rotational transition at 345.795 GHz was detected (Fig. 2) each time we used the SO_2 setting. The spectral line shape for each element depends on the line-of-sight atmospheric temperature profile, local topography, surface-atmosphere temperature difference, and so on. The convolved line shape (Fig. 2) thus depends on viewing geometry, season, time of day, and related factors, and is used to retrieve a representative temperature profile for Mars at the time of the observations. CO is assumed to be well mixed in the vertical and horizontal direction on Mars (Muhleman and Clancy, 1995) and we adopt a constant mixing ratio of 800 ppm (Lellouch et al., 1991). For comparison, Curiosity's Sample Analysis at Mars (SAM) measured atmospheric CO abundance of $<1.0 \times 10^{-3}$ using repeated measurements from Gale crater (4.5°S, 132°E) between solar longitudes 133.7° and 211.2° (Mahaffy et al., 2013).

The method of inverting the CO line is as follows: For each night, we adopted Mars' geometry at the mid-point of each observation interval as representative of the entire interval. We then divided the Mars disk into a grid of 36×36 bins and extracted the temperature–pressure profile above the local surface at the center of each bin from the MCD, extending up to 140 km. Six contribution functions (Fig. 3), calculated from each of these profiles, chosen to peak at roughly equally spaced altitudes, were later used as *a priori* functions (and parameters) in the retrieval of the thermal structure in the atmosphere of Mars. The functions were carefully chosen, with equal frequency resolution offsets close to the line center, and then equally spaced in units of scale heights away from line center, close to the CO line continuum. A non-linear least square fitting algorithm, the Levenberg–Marquardt (Markwardt, 2009) was used to retrieve the temperature profiles by multiplying each of the contribution functions in the *a priori* profiles by a scaling factor, and changing the brightness temperature of Mars.

In order to test the assumption of using the surface geometry at the middle of the observation, we calculated the brightness temperature at the beginning and the end of each night. By comparing these values to the brightness temperature calculated when using the geometry at the middle of the observation, we find the variations to be smaller than 3.5%.

The estimated brightness temperature of the Mars disk (Section 2) is an *a priori* input parameter for the fitting algorithm. This initial guess for the brightness temperature and the thermal profiles aims to prevent the Levenberg–Marquardt algorithm from finding a local minimum that is a good mathematical solution, but not a physically plausible one. The extracted thermal profile for Mars that represents the observed disk of the planet (Fig. 4) is one of the 36×36 retrieved profiles. It leads to a minimum chi-square between the modeled and observed CO line shape. The

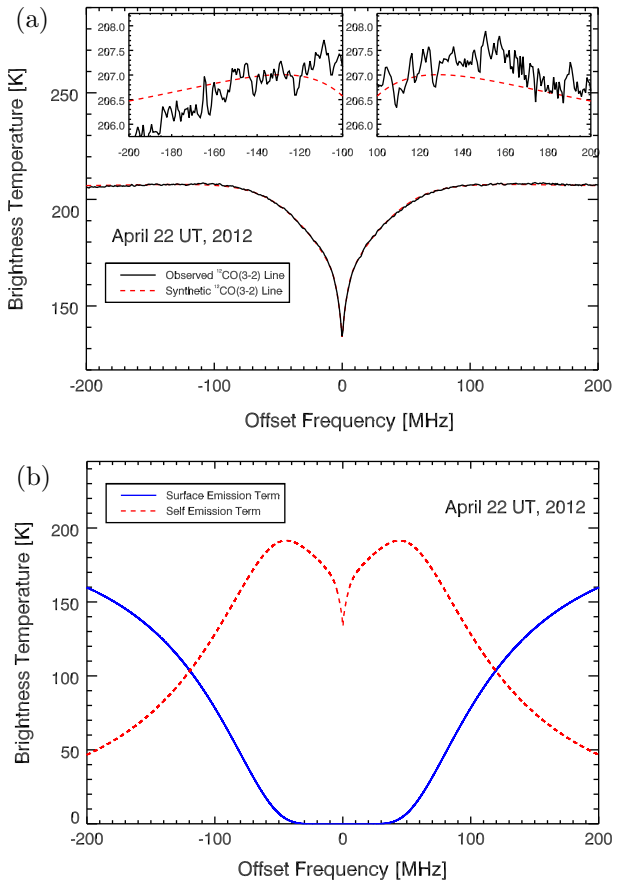

Fig. 2. (a) Observed ^{12}CO(3-2) spectrum of Mars shifted to the rest frequency at 345.796 GHz (solid line) at the retrieved Mars brightness temperature on April 22 UT, 2012. The dashed lines show the synthetic ^{12}CO(3-2) spectrum using the retrieved temperature profile and brightness temperature for Mars at the time of the observation. The inserts show an expanded view of the fit in the wings of the line. (b) Atmospheric self (dashed lines) and surface emission (solid line) terms; their sum is the emergent intensity.

residual spectra resulting from subtracting the model from observed CO, deviate within ±0.7% around zero (Fig. 5). The *a priori* brightness temperatures that we calculated and the retrieved ones from the observations are listed in Table 2.

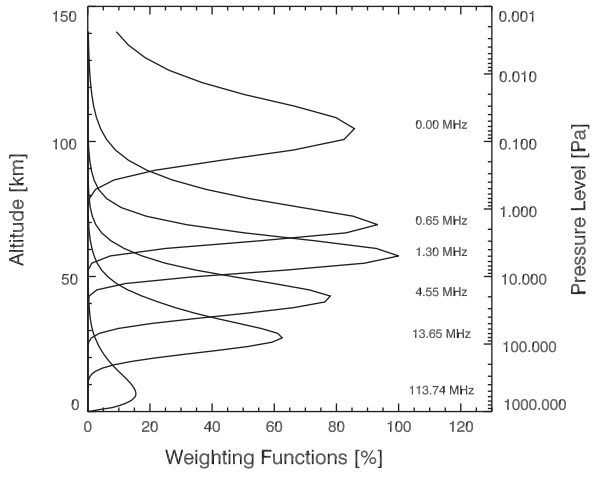

Fig. 3. Contribution functions for the ^{12}CO(3-2) line on April 22 UT, 2012. The frequency offsets where the contribution functions peak from the highest to lowest altitude level are 0, 0.65, 1.3, 4.55, 13.65 and 113.74 MHz.

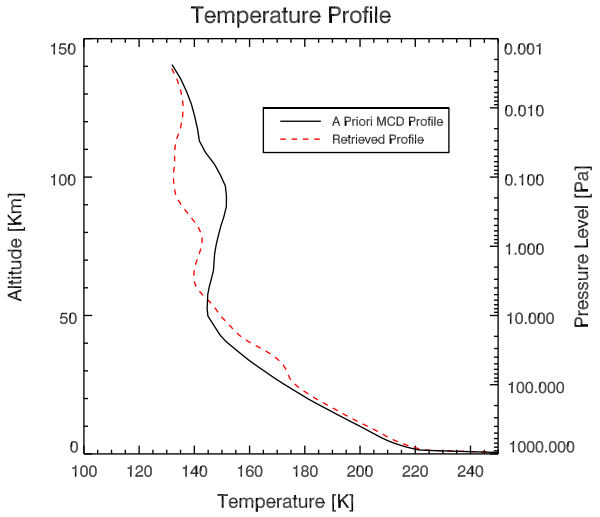

Fig. 4. One of the 36 × 36 *a priori* MCD profiles (solid line) that are used to invert the ^{12}CO(3-2) line. The retrieved temperature profile (dashed lines) leads to the best fit between the observed and synthetic ^{12}CO(3-2) on April 22 UT, 2012, shown in Fig. 2.

The 3.5% uncertainty is on the *a priori* brightness temperatures, and not on the retrieved temperatures that will later be used to calculate the mixing ratios of the sulfur-bearing species.

The extracted temperature profiles and the brightness temperatures for Mars are later used in synthesizing the targeted lines at the time of the observation (Fig. 6). Since the apparent size of Mars is smaller than the diffraction limited field of view of the CSO, the resulting spectra for the different sulfur molecules are disk-averaged.

3.3. Radiative transfer model

In order to synthesize our spectra, we developed a radiative transfer code for computing the expected line absorption. We assume that the sulphuretted species are well mixed, and that the temperature–pressure profile is uniform across Mars. We used an approximation to the entire disk of Mars by assuming a diffusivity factor of 1.66 for our calculations (Encrenaz et al., 2004). In our model, the mixing ratio for each target species is assumed to be uniform across the disk, as is the total surface pressure. For a multi-layered, plane-parallel atmosphere, at normal incidence, the radiative transfer equation is given by the equation for the emerging intensity:

$$I_\nu = \epsilon_0 B_\nu(T_s) e^{-\tau_{0,\nu}} + \int_0^{\tau_{0,\nu}} B_\nu(T) e^{-\tau_\nu(z)} d(\tau_\nu(z)) \quad (4)$$

where ϵ_0 is the emissivity of the surface of Mars at the observed frequency ($\epsilon_0 = 0.96$), B_ν is the Planck function, T_s is the surface temperature of Mars, $T = T(z)$ is the temperature at each layer at altitude z, $\tau_\nu(z)$ is the frequency-dependent optical depth above each layer at altitude z, and $\tau_{0,\nu}$ is the total optical depth of the atmosphere.

At the Rayleigh–Jeans approximation of Planck's law, the radiative transfer equation becomes:

$$T_\nu = \epsilon_0 T_s e^{-\tau_{0,\nu}} + \int_0^{\tau_{0,\nu}} T(z) e^{-\tau_\nu(z)} d(\tau_\nu(z)) \quad (5)$$

where T_ν is the frequency-dependent flux in units of brightness temperature. The optical path increases with the incidence angle, and therefore the optical depth is multiplied by the factor $1/\mu = \sec(\theta)$. In our calculation, we use the effective zenith angle

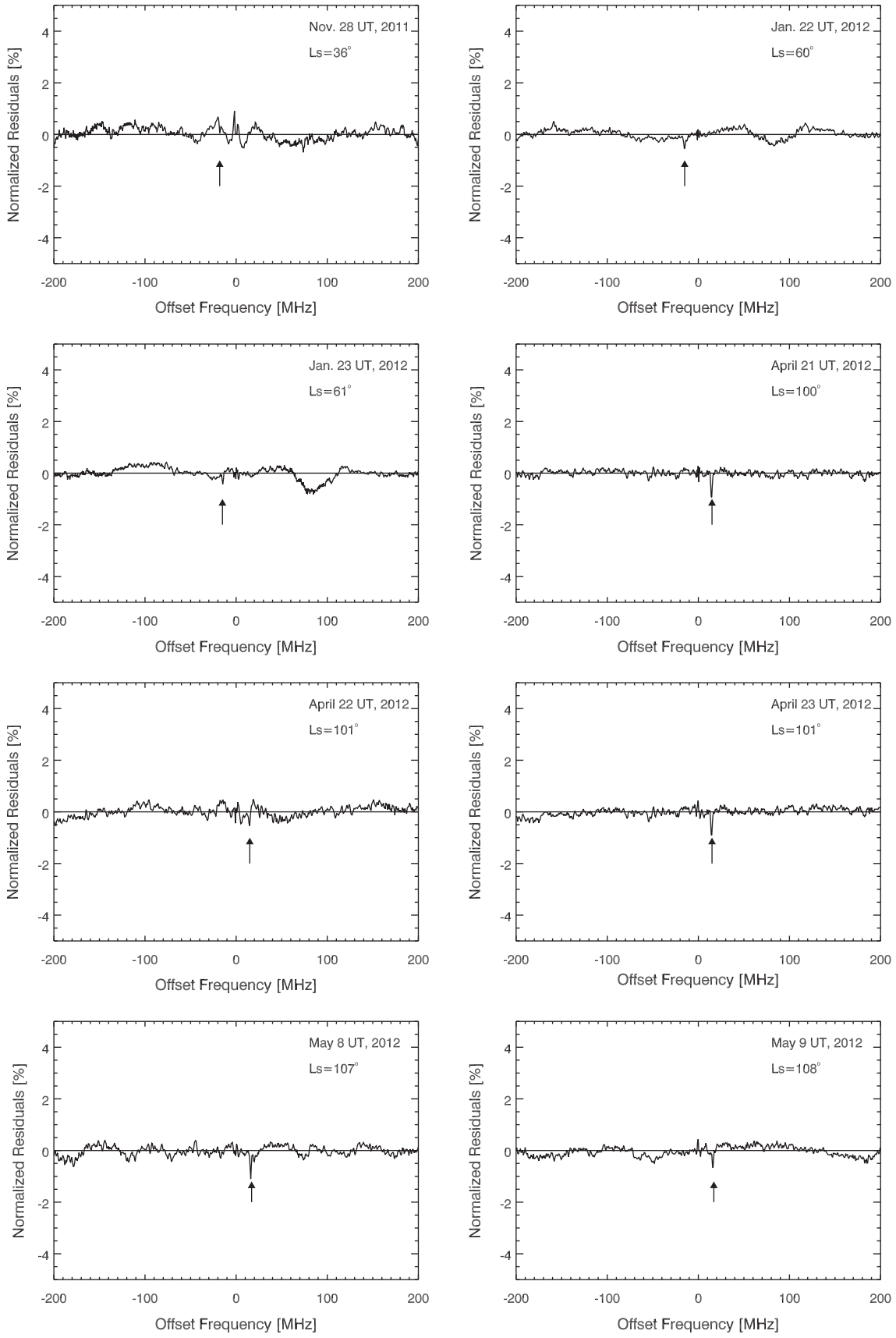

Fig. 5. Residual spectra showing the difference between the observed and synthetic ^{12}CO(3-2), normalized to the continuum of Mars at different observing dates. Arrow indicates the position of the telluric ^{12}CO(3-2) line.

Table 2
Calculated and retrieved brightness temperatures for the disk-averaged surface of Mars between 28 November 2011 and 9 May 2012 (L_s = 36–108°).

Date (UT)	T_b (K)	Retrieved T_b (K)	L_s (°)
28 November 2011	217.79	206.51	36.00
22 January 2012	226.33	211.22	60.40
23 January 2012	226.28	208.93	60.85
21 April 2012	213.86	203.60	99.84
22 April 2012	211.75	204.86	100.29
23 April 2012	211.56	210.39	100.75
8 May 2012	214.34	203.83	107.53
9 May 2012	214.45	209.33	107.96

(θ = 53°), leading to an airmass of $1/\bar{\mu}$ = 1.66. The opacity above each layer at altitude z in the atmosphere is given by:

$$\tau_v(z) = \int_z^{\infty} \alpha_v(z') \frac{dz'}{\bar{\mu}} \tag{6}$$

where $\alpha_v(z')$ is the absorption coefficient at each layer at altitude z ($z > z'$), and $d(z')$ is its corresponding thickness. The atmospheric layers are chosen to have an increasing thickness in the direction of altitude.

The absorption coefficient at each layer of the atmosphere, as a function of frequency is given by:

$$\alpha_v(z) = S_v(T) \times N(z) \times f_v(v - v_0). \tag{7}$$

where $S_v(T)$ is the strength of the transition, $N(z)$ is the number density of the analyzed constituent in the atmosphere contained in each layer, and is expressed as:

$$N(z) = \frac{q \times P(z)}{k_B \times T(z)} \tag{8}$$

$P(z)$ is the pressure at altitude z of the atmospheric layer, q is the volume mixing ratio of the molecule analyzed. We consider a well mixed atmosphere where the mixing ratio is constant with altitude and k_B is the Boltzmann constant. $f_v(v - v_0)$ is the frequency-dependent normalized Voigt function. In the pressure-broadened profile, γ, the half width of the Lorentzian should be calculated by:

$$\gamma = \gamma_f \times \frac{P}{P_0} \times (1 - q) \times \left(\frac{T_0}{T}\right)^{n_f} + A \tag{9}$$

$$A = \gamma_s \times \frac{P}{P_0} \times q \times \left(\frac{T_0}{T}\right)^{n_s} \tag{10}$$

P_0 and T_0 are the pressure and temperature at the reference standard temperature and pressure (STP), P and T are the pressure and temperature at each atmospheric layer, γ_f and γ_s are the foreign and self broadened Lorentz half widths, whereas n_f and n_s are the temperature dependent coefficients for the foreign and self broadening coefficients, respectively. In the martian atmosphere, the molecules are considered under a CO_2 collisional regime. Therefore we used for CO(3-2) the following pressure-broadening constants: γ_{CO-CO_2} = 0.116, γ_{CO-CO} = 0.079 (Belov et al., 1992), n_{CO-CO_2} = 0.75 (Varanasi, 1975) and n_{CO-CO} = 0.74 (Rothman et al., 2009).

4. Results

The data were processed using the Line Analysis Single-dish Software (CLASS)[5] and our own developed data reduction and analysis pipeline, coded in IDL (Exelis Visual Information Solutions, Boulder, Colorado). For each scan during each night, the baseline was corrected using polynomial fitting (degree 8), then aligned based on the velocity (Doppler) shift. After summing up the spectra for one night, the baseline around line center was corrected using polynomial fitting of degree 3 (Fig. 1). The reciprocal square of the corresponding RMS at the continuum was used as a weighting factor, when summing up the spectra over time during one night, and over different nights. The double side band spectrum was converted into a single side spectrum after removing the continuum contribution from the lower side band. Taking into account the beam efficiency of the telescope, the angular size of Mars and the telescope's beam width at the frequency setting, we then normalized the single side band spectrum to the retrieved continuum of Mars at the time of each observation.

We applied our radiative transfer model to synthesize each spectral line, with the appropriate line shape parameters in a CO_2 collisional atmosphere (with 95% CO_2). The foreign broadening coefficients for SO_2 and H_2S are 0.18 cm^{-1}/atm (Suleiman et al., 1996) and 0.13 cm^{-1}/atm (Kissel et al., 2002), respectively. For SO, the broadening coefficient is not measured but we assumed it is 1.3 times larger than in air, or 4 MHz/torr (0.10 cm^{-1}/atm). The dependence of the transition strength on temperature is taken into account by implementing the appropriate partition functions. The spectral lines are modeled at a spectral resolution of $\sim 7 \times 10^{-3}$ MHz, then convolved with a boxcar kernel of 1 MHz width, the spectral resolution of the spectrometer. We later interpolated these values with the channel spacing of 0.65 MHz in order to compare our synthetic line shapes with the combined measured spectrum.

In order to calculate the photochemical lifetimes of the targeted molecules in the atmosphere of Mars, a photochemical model is required. Krasnopolsky et al. (2004) noted that it requires 0.5 years for molecules to be well mixed in the atmosphere of Mars. This timescale is shorter than the calculated 2 years lifetime for SO_2 (Krasnopolsky, 1995; Nair et al., 1994). Therefore, SO_2 is assumed to be well mixed across the disk of the planet. If we consider a steady state outgassing event for SO_2 we can combine the spectra of this molecule independently for all the observing runs from November 2011 ($L_s = 34°$) until May 2012 ($L_s = 110°$). We cannot do the same for H_2S and SO due to the shorter photochemical lifetimes than the timespan between the observing runs, and therefore each observing night is treated individually. None of these sulfur species is condensible at the pressure and temperature conditions present on Mars, even in the polar regions.

When modeling the SO_2 spectral line that we compare against the co-added spectrum, we applied the same weighting factor we used before when co-adding the data. It is the reciprocal square of the corresponding RMS at the continuum of each spectrum at each night. This same weighting factor is used to average the temperature–pressure profile, the surface temperature, and the surface pressure extracted for each night. The weighted-averaged atmospheric parameters are then used to model the long term average SO_2 line.

The co-added spectrum of SO_2, and the spectra of SO and H_2S on the best nights of 11 May and 21 January, 2012, respectively are displayed in Fig. 7. The spectrum for each species is shown as a solid line with error bars. The spectrum is normalized to the continuum of Mars and shifted to the rest frequency. The dashed lines are the expected absorption for each molecule at the 2σ and 3σ levels, where an upper limit at 2σ level corresponds to a line depth that is two standard deviations from the continuum. We do not see any absorption line for SO_2, SO or H_2S. For total integration time of 9.33 h, the RMS noise level (one standard deviation) in the co-added spectrum is 0.0165% for SO_2. For the integration times of 50 mn and 97 mn on 11 May and 21 January, 2012, respectively, the RMS noise levels in the spectra are 0.0495% for SO and 0.0367% for H_2S. A summary of our results is presented in Table 3.

[5] http://www.iram.fr/IRAMFR/GILDAS.

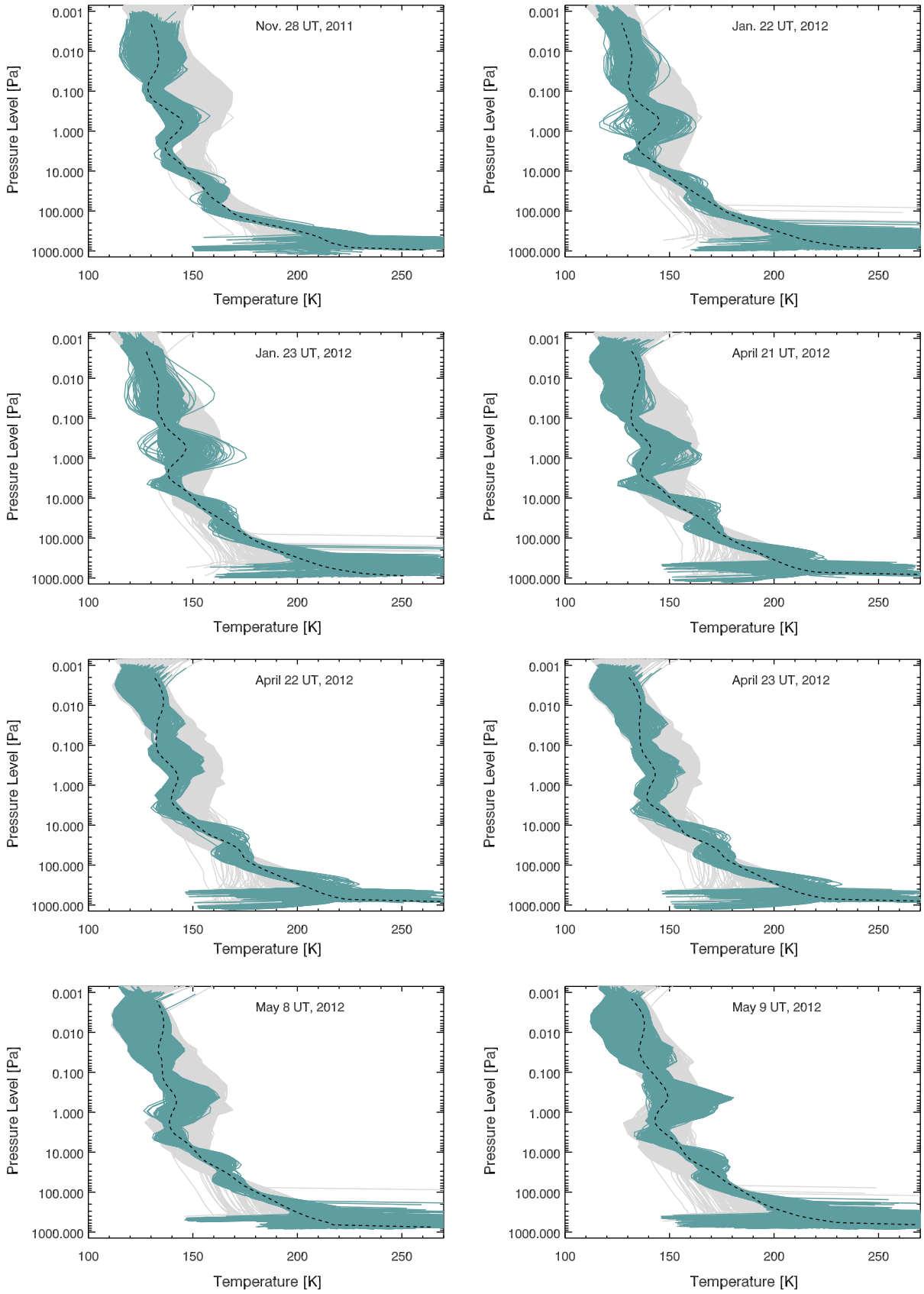

Fig. 6. For each night on which CO is observed, we show 36 × 36 *a priori* MCD profiles (gray lines), the retrieved temperature profiles (turquoise lines), and the optimum extracted profile for calculating the abundance of the sulfur species (dashed black line).

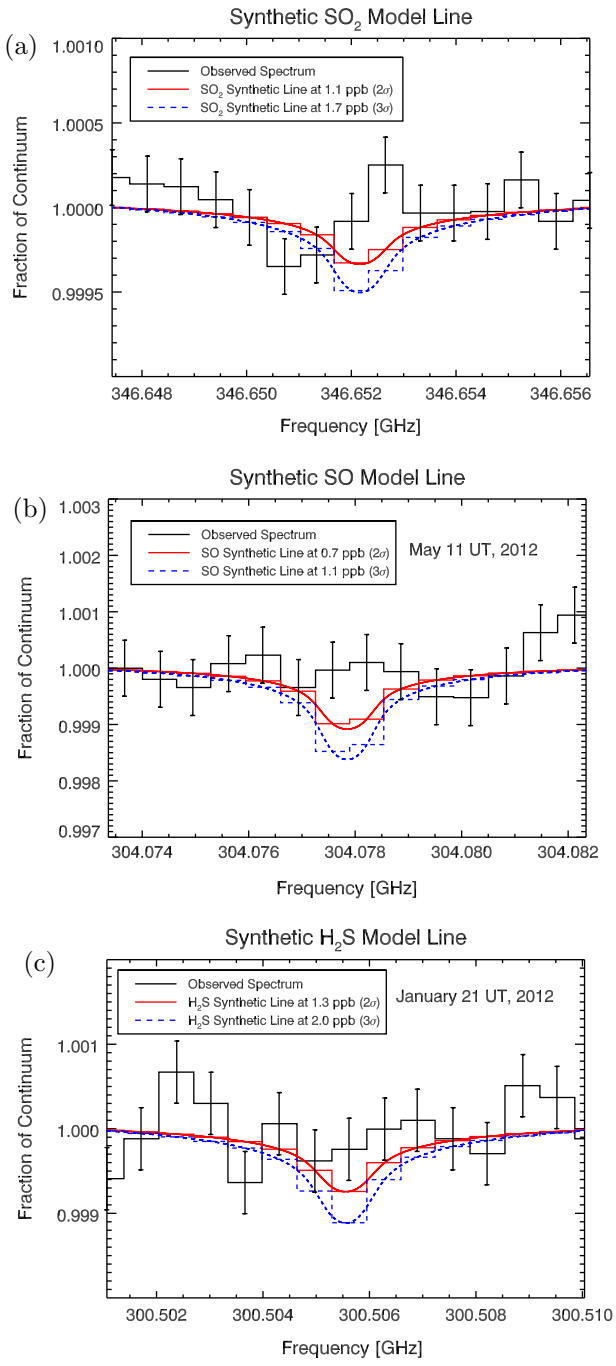

Fig. 7. The black solid line shows the spectrum for SO_2, SO and H_2S. For SO_2, it is the co-added spectrum for all the observing nights, while for SO and H_2S, it is the spectrum on the best night. The spectra are normalized to the continuum of Mars and shifted to the rest frequency. The red solid line and the dashed blue lines show the expected absorption at 2σ and 3σ, respectively.

Although the continuum level is uncertain by ±15%, the equivalent width of the spectral lines is conserved, and therefore this 15% uncertainty does not affect the retrieved upper limit on the mixing ratios.

Our upper limit for SO_2 is consistent with previous limits by Krasnopolsky (2012), Encrenaz et al. (2011) and Nakagawa et al. (2009), and is the most sensitive obtained in submillimeter wavelengths (see Table 3). Our value for the H_2S upper limit is 15 times smaller than the upper limit retrieved at millimeter wavelengths by Encrenaz et al. (1991), due to the facts that the transition at 300.505 GHz is 5 times stronger than that at 216.716 GHz, and the longer on-source integration spent to collect the spectra.

5. Discussion

Our upper limit on SO_2 of 1.1 ppb corresponds to a total mass of 40 ktons of SO_2 uniformly distributed across the atmosphere of Mars. In Earth's volcanoes, the amount of SO_2 released is generally $1–10^5$ times that of methane (CH_4) (Delmelle and Stix, 2000; Nakagawa et al., 2009).

In the case of an ongoing outgassing and a lifetime of 2 years for SO_2, the total abundance of SO_2 in the atmosphere should be invariant and globally distributed. If we assume ongoing outgassing at the time when Mumma et al. (2009) detected CH_4, then we would expect 1.1–0.01 ppt of methane, if outgassed solely from volcanoes. The expected abundance is then lower than what was measured (6 ppb), and so the methane released could not have a (mainly) volcanic origin when considering terrestrial SO_2/CH_4 outgassing ratios and continuous outgassing.

In the case of a one-time outgassing event of SO_2 and CH_4 at the time when Mumma et al. (2009) detected methane, then the amount of SO_2 should decay exponentially with the lifetime of 2 years between 2003 and 2012. After 9 years, only 1% of the original SO_2 should be detectable. This upper limit of 40 ktons in 2012 would correspond to 3600 ktons of SO_2 in 2003. Mumma et al. (2009) detected 42 ktons of CH_4, and using the SO_2/CH_4 ratio in terrestrial volcanoes, the measured methane abundance is within the expected range, but our SO_2 limit of 2012 does not allow to differentiate the origin of the observed CH_4 when considering sporadic release.

When considering the earlier searches for SO_2 by Krasnopolsky (2005, 2012), Nakagawa et al. (2009), and Encrenaz et al. (2011), and a stringent limit of 0.3 ppb (11 ktons) just 2–3 months after the release, the methane release observed by Mumma et al. (2009) could not be of (mainly) volcanic origin when considering terrestrial SO_2/CH_4 outgassing ratios.

Our current upper limit of 1.1 ppb, combined with a lifetime of SO_2 of 2 years, yields an outgassing rate of SO_2 of less than 55 metric tons/day (t/d), if a release is steady. Kilauea (Hawaii) and Masaya (Nicaragua) volcanoes are considered as terrestrial analogs to the Tharsis volcanoes (Mouginis-Mark et al., 2007), with an average SO_2 emission rate of 1650 t/d for Kilauea (Elias and Sutton, 2012), and 1100 t/d for Masaya (William-Jones et al., 2003). Average values for the measured SO_2 outgassing rates (t/d) for some Earth volcanoes compared to our derived upper limit on the rate for Mars are presented in Table 4.

If we assume that perhaps there is still active volcanism within the crust, then measuring SO_2 fluxes is not only a good indicator for volcanic activity, but it also serves in estimating the amount of the magma that degassed the SO_2, if all the sulfur dioxide originates from the magma (Andres et al., 1991; Kazahaya et al., 1994). The mechanism for releasing SO_2 is described by the *Poiseuille* flow model, occurring at the upper part of the magma body, where the magma transport is driven by buoyancy. The difference in density between the non-degassed, lower density magma, and the degassed, higher density magma, drives the former to ascend in the inner part of the conduit, and the latter to descend in the outer part (Kazahaya et al., 1994). The non-degassed magma, reaching the top of the magma body, releases the SO_2. The mass rate of magma degassing Q (kg/s) is related to the outgassed SO_2 flux by Kazahaya et al. (1994):

$$Q = \frac{M_S Q_{SO_2}}{M_{SO_2} \Delta C_S} \tag{11}$$

Table 3
Abundance limits (2σ) for the sulphuretted species on Mars.

Molecule	Date (UT)	This work (ppb)	Previous (ppb)	Reference
SO	11 May 2012	0.7	–	–
H_2S	21 January 2012	1.3	20 (in the mm)	Encrenaz et al. (1991)
SO_2	co-added over all nights	1.1	0.3 (in the IR)	Krasnopolsky (2012) and Encrenaz et al. (2011)
SO_2	co-added over all nights	1.1	2.0 (in the submm)	Nakagawa et al. (2009)
SO_2	28 November 2011	5.7		
SO_2	22 January 2012	2.0		
SO_2	23 January 2012	2.3		
SO_2	21 April 2012	4.3		
SO_2	22 April 2012	5.6		
SO_2	23 April 2012	2.4		
SO_2	08 May 2012	3.2		
SO_2	09 May 2012	5.4		
SO	27 November 2011	1.2		
SO	18 January 2012	1.8		
SO	19 January 2012	0.9		
SO	20 April 2012	1.7		
SO	24 April 2012	0.9		
SO	10 May 2012	0.9		
H_2S	29 November 2011	4.1		
H_2S	20 January 2012	1.5		
H_2S	25 April 2012	3.1		
H_2S	26 April 2012	1.8		
H_2S	12 May 2012	3.7		
H_2S	13 May 2012	3.0		

Table 4
Average values for the measured SO_2 outgassing rates for some Earth volcanoes compared to our derived rate for Mars.

Volcano	Average SO_2 flux (metric tons/day)	Period over which the measurements were obtained	Reference
This work for Mars	$\leqslant$55	Assuming constant outgassing	
Kilauea (Hawaii)	1650	1979–2010	Elias and Sutton (2012)
Masaya (Nicaragua)	1100	1993–2001	William-Jones et al. (2003)
Nyamuragira (Congo)	$\geqslant$2600	1979–2005	Bluth and Carn (2008)
Sierra Negra (Ecuador)	11	July 2006	Barrancos et al. (2008)
Erebus (Antarctica)	46	2 h on 26 December 2006	Boichu et al. (2010)
Erta 'Ale (Ethiopia)	60	1 h on 15 October 2005	Sawyer et al. (2008)

where Q_{SO_2} is the outgassing rate of SO_2 (kg/s), M_S and M_{SO_2} are the molar weights for S and SO_2, respectively, and ΔC_S is the sulfur content of the degassing magma. Theoretical models by Gaillard and Scaillet (2009) denote values of 600–900 ppm (average 750 ppm) for the sulfur content in the mantle of Mars. With our retrieved upper limit for SO_2 of 55 t/day (0.64 kg/s), and a density of 2600 kg/m^3 for the basalt magma (Spera, 2000), the upper limit on the mass rate of magma that is able to degass SO_2 is 37 ktons/day (425 kg/s), or 12,000 m^3/day (0.14 m^3/s).

Leshin et al. (2013) reported the presence of SO_2 and H_2S among the evolved gases when heating samples (up to ~1108 K) of the Rocknest aeolian deposit at the site of the Mars Curiosity Rover. A possible origin of these sulfur species is the breakdown of S bearing minerals trapped in the solid phase. This suggests that the release of SO_2 and H_2S is possible at high temperatures, a characteristic of volcanic events. Along with establishing an upper limit on SO, our current limit on H_2S is a significant improvement over previous limits, and limits the presence of major current outgassing events on Mars, and puts constraints on the photochemistry in the martian atmosphere.

Our multi-species survey at two different seasons on Mars took advantage of a high spectral resolving power to look for major outgassing across the disk of the planet, but there are limitations to what single dish antennae could offer in terms of spatial resolution. The next step would be to spatially resolve the planet using the Atacama Large Millimeter Array (ALMA) and be able to search for localized and temporal outgassing events. Since SO_2 is the strongest indicator for volcanic outgassing as it is the most abundant among the other sulfur species in terrestrial analog volcanoes (Symonds et al., 1994), a good strategy would be to only target SO_2 at the sub-millimeter at different locations and seasons on Mars. The detection of atmospheric SO_2 would be a powerful indicator to trigger the search for H_2S and SO.

6. Summary

With ground-based high-resolution submillimeter spectroscopy, we searched for active release of gases on Mars during 23 November 2011–13 May 2012 which corresponded to its mid Northern Spring and early Northern Summer seasons ($L_s = 34$–110°). The targeted volcanic areas, Tharsis and Syrtis Major were observed using the heterodyne receiver (Barney) at the 10.4 m Caltech Submillimeter Observatory (CSO) on Mauna Kea, Hawaii. Our survey targeted sulfur dioxide (SO_2), sulfur monoxide (SO) and hydrogen sulfide (H_2S) at their rotational transitions at 346.652 GHz, 304.078 GHz and 300.505 GHz, respectively. No active release was detected, and we infer 2σ upper limits across the disk of the planet of 1.1 ppb, 0.7 ppb and 1.3 ppb for SO_2, SO and H_2S, respectively.

By estimating methane abundances that could be released as a result of volcanic outgassing using the ratio of SO_2/CH_4 in terrestrial volcanoes, we conclude a non-volcanic origin for the methane released in 2003 if an ongoing outgassing of SO_2 occurred. In the case of a one-time outgassing event of SO_2 and CH_4 at the time when Mumma et al. (2009) detected methane, we cannot draw conclusions on the origin of the CH_4 released.

Our current upper limit of 1.1 ppb for SO_2 yields an outgassing rate of less than 55 metric tons/day. Compared to two terrestrial analogs, we would be able to detect any volcanic release that is more than 4% the size of Kilauea or one twentieth the size of the Masaya volcano. The mass rate of magma that is able to degas 55 tons of SO_2 per day is 37 ktons of magma per day, or 12,000 m^3 per day. The non-detection of any of the sulfur compounds in the atmosphere of Mars indicates the absence of major volcanic outgassing, and provides limits for the level of current volcanic activity in the crust of Mars.

Future observations with ALMA will take advantage of its unprecedented sensitivity at sub arc-second spatial resolutions on Mars. Searching for temporal outgassing of different sulphuretted species from localized sources on the planet will be then possible.

Acknowledgments

We are grateful to the staff at the Caltech Submillimeter Observatory (CSO), Simon Radford, Timm Riesen and Louis Scuderi for their support during the Mars observing runs. This material is based upon work at the CSO, which is operated by the California Institute of Technology under cooperative agreement with the National Science Foundation, Grant No. AST-0838261. We gratefully acknowledge the support from the NASA Planetary Astronomy Program under Cooperative Agreement NNX08AE38A, NASA contract NNH14CK55B, RTOP 344-32-07 and NASA's Astrobiology Program (RTOP 344-53-51) that supported M.J.M., and G.L.V. A.J.K. would like to thank Norbert Schörghofer who provided valuable ideas to the writing and undertaking of the research summarized here. The authors wish to recognize and acknowledge the very significant cultural role and reverence that the summit of Maunakea has always had within the indigenous Hawaiian community. We are most fortunate to have the opportunity to conduct observations from this mountain.

References

Andres, R.J. et al., 1991. Excessive sulfur dioxide emissions from Chilean volcanoes. J. Volc. Geotherm. Res. 46, 323–329.

Barrancos, J. et al., 2008. SO_2 emission from active volcanoes measured simultaneously by COSPEC and mini-DOAS. In: Pérez, N., Gurrieri, S., King, C.Y., Taran, Y. (Eds.), Terrestrial Fluids, Earthquakes and Volcanoes: The Hiroshi Wakita, Pageoph Topical Volumes, vol. III. Birkhäuser, Basel, pp. 115–133. http://dx.doi.org/10.1007/978-3-7643-8738-9_8.

Belov, S.P., Tretiakov, M.I., Suenram, R.D., 1992. Improved laboratory rest frequency measurements and pressure shift and broadening parameters for the J = 2–1 and J = 3–2 rotational transitions of CO. Astrophys. J. 393, 848–851. http://dx.doi.org/10.1086/171551.

Bluth, G.J.S., Carn, S.A., 2008. Exceptional sulfur degassing from Nyamuragira volcano, 1979–2005. Int. J. Remote Sens. 29, 6667–6685. http://dx.doi.org/10.1080/01431160802168434.

Boichu, M. et al., 2010. High temporal resolution SO_2 flux measurements at Erebus volcano, Antarctica. J. Volc. Geotherm. Res. 190, 325–336. http://dx.doi.org/10.1016/j.jvolgeores.2009.11.020, <http://www.sciencedirect.com/science/article/pii/S0377027309004569>.

Christensen, P.R. et al., 2001. Mars Global Surveyor Thermal Emission Spectrometer experiment: Investigation description and surface science results. J. Geophys. Res. 106, 23823–23872. http://dx.doi.org/10.1029/2000JE001370.

Delmelle, P., Stix, J., 2000. Volcanic Gases. In: Sigurdsson, H. (Ed.), Encyclopedia of Volcanoes. Academic Press, San Diego, pp. 803–815.

Edgett, K.S., et al., 2010. Active and recent volcanism and hydrogeothermal activity on Mars. In: AAS/Division for Planet. Sci. Meeting Abstracts #42, p. 1016.

Elias, T., Sutton, A., 2012. Sulfur Dioxide Emission Rates from Kilauea Volcano, Hawai'i, 20072010. U.S. Geological Survey Open-File Report 2012-1107, pp. 1–25, <http://pubs.usgs.gov/of/1998/of98-462/>.

Encrenaz, T. et al., 1991. The atmospheric composition of Mars – ISM and ground-based observational data. Ann. Geophys. 9, 797–803.

Encrenaz, T. et al., 1995. Detectability of molecular species in planetary and satellite atmospheres from their rotational transitions. Planet. Space Sci. 43, 1485–1516. http://dx.doi.org/10.1016/0032-0633(95)00064-X.

Encrenaz, T. et al., 2004. Detectability of minor constituents in the martian atmosphere by infrared and submillimeter spectroscopy. Planet. Space Sci. 52, 1023–1037. http://dx.doi.org/10.1016/j.pss.2004.07.011.

Encrenaz, T. et al., 2011. A stringent upper limit to SO_2 in the martian atmosphere. Astron. Astrophys. 530, A37. http://dx.doi.org/10.1051/0004-6361/201116820.

Forget, F. et al., 1999. Improved general circulation models of the martian atmosphere from the surface to above 80 km. J. Geophys. Res. 104, 24155–24176. http://dx.doi.org/10.1029/1999JE001025.

Frankel, C., 1996. Volcanoes of the Solar System. Cambridge University Press.

Gaillard, F., Scaillet, B., 2009. The sulfur content of volcanic gases on Mars. Earth Planet. Sci. Lett. 279, 34–43. http://dx.doi.org/10.1016/j.epsl.2008.12.028.

Golombek, M.P., et al., 2008. Martian surface properties from joint analysis of orbital, Earth-based, and surface observations. In: Bell III, J. (Ed.), The martian Surface – Composition, Mineralogy, and Physical Properties, p. 468.

Hartmann, W.K. et al., 1999. Evidence for recent volcanism on Mars from crater counts. Nature 397, 586–589. http://dx.doi.org/10.1038/17545.

Hauber, E., Brož, P., Jagert, F., 2010. Plains volcanism on Mars: Ages and rheology of lavas. Lunar Planet. Sci. p. 1298 (abstract).

Horn, J. et al., 1999. A 4 × 1 GHz array acousto-optical spectrometer. Exp. Astron. 9, 17–38.

Kazahaya, K., Shinohara, H., Saito, G., 1994. Excessive degassing of izu-oshima volcano: Magma convection in a conduit. B. Volcanol. 56, 207–216. http://dx.doi.org/10.1007/BF00279605, <http://dx.doi.org/10.1007/BF00279605>.

Kissel, A. et al., 2002. Molecular-gas-pressure-induced line-shift and line-broadening in the v_2-band of H_2S. J. Mol. Spectrosc. 216, 345–354. http://dx.doi.org/10.1006/jmsp.2002.8630.

Kooi, J.W. et al., 2007. A 275–425-GHz Tunerless waveguide receiver based on AlN-barrier SIS technology. IEEE Trans. Microw. Theory Tech. 55, 2086–2096. http://dx.doi.org/10.1109/TMTT.2007.905503.

Krasnopolsky, V.A., 1995. Uniqueness of a solution of a steady state photochemical problem: Applications to Mars. J. Geophys. Res. 100, 3263–3276. http://dx.doi.org/10.1029/94JE03283.

Krasnopolsky, V.A., 2005. A sensitive search for SO_2 in the martian atmosphere: Implications for seepage and origin of methane. Icarus 178, 487–492. http://dx.doi.org/10.1016/j.icarus.2005.05.006.

Krasnopolsky, V.A., 2012. Search for methane and upper limits to ethane and SO_2 on Mars. Icarus 217, 144–152. http://dx.doi.org/10.1016/j.icarus.2011.10.019.

Krasnopolsky, V.A., Maillard, J.P., Owen, T.C., 2004. Detection of methane in the martian atmosphere: Evidence for life? Icarus 172, 537–547. http://dx.doi.org/10.1016/j.icarus.2004.07.004.

Lellouch, E. et al., 1991. First absolute wind measurements in the middle atmosphere of Mars. Astrophys. J. 383, 401–406. http://dx.doi.org/10.1086/170797.

Leshin, L.A. et al., 2013. Volatile, isotope, and organic analysis of martian fines with the Mars Curiosity rover. Science 341, 1238937-1–1238937-9.

Lewis, S.R. et al., 1999. A climate database for Mars. J. Geophys. Res. 104, 24177–24194. http://dx.doi.org/10.1029/1999JE001024.

Mahaffy, P.R. et al., 2013. Abundance and isotopic composition of gases in the martian atmosphere from the Curiosity rover. Science 341, 263–266.

Markwardt, C.B., 2009. Non-linear least-squares Fitting in IDL with MPFIT. In: Bohlender, D.A., Durand, D., Dowler, P. (Eds.), Astron. Data Anal. Softw. Syst. XVIII, p. 251. 0902.2850.

Matthews, H.E., Leech, J., Friberg, P., 2004. Guide to Spectral Line Observing at the JCMT. <http://cso.caltech.edu/wiki/cso/instruments/heterodyne/pointing>.

Mouginis-Mark, P.J., Harris, A.J., Rowland, S.K., 2007. Terrestrial analogs to the calderas of the tharsis volcanoes on Mars. In: The Geology of Mars. Cambridge University Press, pp. 71–94. http://dx.doi.org/10.1017/CBO9780511536014.004.

Muhleman, D.O., Clancy, R.T., 1995. Microwave spectroscopy of the Mars atmosphere. Appl. Opt. 34, 6067. http://dx.doi.org/10.1364/AO.34.006067.

Mumma, M.J. et al., 2009. Strong release of methane on Mars in northern summer 2003. Science 323, 1041–1045. http://dx.doi.org/10.1126/science.1165243.

Nair, H. et al., 1994. A photochemical model of the martian atmosphere. Icarus 111, 124–150. http://dx.doi.org/10.1006/icar.1994.1137.

Nakagawa, H. et al., 2009. Search of SO_2 in the martian atmosphere by ground-based submillimeter observation. Planet. Space Sci. 57, 2123–2127. http://dx.doi.org/10.1016/j.pss.2009.10.001.

Neukum, G. et al., 2004. Recent and episodic volcanic and glacial activity on Mars revealed by the High Resolution Stereo Camera. Nature 432, 971–979. http://dx.doi.org/10.1038/nature03231.

Oppenheimer, C., Scaillet, B., Martin, R.S., 2011. Sulfur degassing from volcanoes: Source conditions, surveillance, plume chemistry and Earth system impacts. Rev. Min. Geochem. 73, 363–421.

Penzias, A.A., Burrus, C.A., 1973. Millimeter-wavelength radio-astronomy techniques. Annu. Rev. Astron. Astrophys. 11, 51. http://dx.doi.org/10.1146/annurev.aa.11.090173.000411.

Pickett, H.M. et al., 1998. Submillimeter, millimeter and microwave spectral line catalog. J. Quant. Spectrosc. Radiat. Trans. 60, 883–890. http://dx.doi.org/10.1016/S0022-4073(98)00091-0.

Robbins, S.J., Achille, G.D., Hynek, B.M., 2011. The volcanic history of Mars: High-resolution crater-based studies of the calderas of 20 volcanoes. Icarus 211, 1179–1203. http://dx.doi.org/10.1016/j.icarus.2010.11.012.

Rothman, L.S. et al., 2009. The HITRAN 2008 molecular spectroscopic database. J. Quant. Spectrosc. Radiat. Trans. 110, 533–572. http://dx.doi.org/10.1016/j.jqsrt.2009.02.013.

Sawyer, G.M. et al., 2008. Magmatic degassing at Erta 'Ale volcano, Ethiopia. J. Volc. Geotherm. Res. 178, 837–846. http://dx.doi.org/10.1016/j.jvolgeores.2008.09.017.

Schilke, P. et al., 1997. A line survey of orion KL from 325 to 360 GHz. Astrophys. J. Suppl. Ser. 108, 301. http://dx.doi.org/10.1086/312948.

Simpson, R.A., et al., 1992. Radar determination of Mars surface properties. In: Kieffer, H.H., Jakosky, B.M., Snyder, C.W., Matthews, M.S. (Eds.), Mars, pp. 652–685.

Spera, F.J., 2000. Physical properties of magma. In: Encyclopedia of Volcanoes, pp. 171–190.

Suleiman, S.H., Kolodner, M.A., Steffes, P.G., 1996. Laboratory measurement of the temperature dependence of gaseous sulfur dioxide (SO_2) microwave absorption with application to the Venus atmosphere. J. Geophys. Res. 101, 4623–4636. http://dx.doi.org/10.1029/95JE03728.

Symonds, R. et al., 1994. Volcanic-gas studies: Methods, results and applications. Volatiles Magmas: Miner. Soc. Am. Rev. Miner. 30, 1–66.

Varanasi, P., 1975. Measurement of line widths of CO of planetary interest at low temperatures. J. Quant. Spectrosc. Radiat. Trans. 15, 191–196. http://dx.doi.org/10.1016/0022-4073(75)90017-5.

Werner, S.C., 2009. The global martian volcanic evolutionary history. Icarus 201, 44–68. http://dx.doi.org/10.1016/j.icarus.2008.12.019.

William-Jones, G., Rymer, H., Rothery, D.A., 2003. Gravity changes and passive SO_2 degassing at the Masaya caldera complex, Nicaragua. J. Volc. Geotherm. Res. 123, 137–160. http://dx.doi.org/10.1016/S0377-0273(03)00033-7.

Wong, A.S., Atreya, S.K., Encrenaz, T., 2003. Chemical markers of possible hot spots on Mars. J. Geophys. Res. 108, 5026. http://dx.doi.org/10.1029/2002JE002003.

Wong, A.S., Atreya, S.K., Encrenaz, T., 2004. Correction to "Chemical markers of possible hot spots on Mars. J. Geophys. Res. 109, 1007. http://dx.doi.org/10.1029/2003JE002210.

Wong, A.S., Atreya, S.K., Encrenaz, T., 2005. Correction to and updated reaction in "Chemical markers of possible hot spots on Mars". J. Geophys. Res. 110, 10002. http://dx.doi.org/10.1029/2005JE002509.